



LAWRENCE  
LIVERMORE  
NATIONAL  
LABORATORY

# Ignition and Growth Reactive Flow Model for IMX-101

C. M. Tarver

February 19, 2016

## **Disclaimer**

---

This document was prepared as an account of work sponsored by an agency of the United States government. Neither the United States government nor Lawrence Livermore National Security, LLC, nor any of their employees makes any warranty, expressed or implied, or assumes any legal liability or responsibility for the accuracy, completeness, or usefulness of any information, apparatus, product, or process disclosed, or represents that its use would not infringe privately owned rights. Reference herein to any specific commercial product, process, or service by trade name, trademark, manufacturer, or otherwise does not necessarily constitute or imply its endorsement, recommendation, or favoring by the United States government or Lawrence Livermore National Security, LLC. The views and opinions of authors expressed herein do not necessarily state or reflect those of the United States government or Lawrence Livermore National Security, LLC, and shall not be used for advertising or product endorsement purposes.

This work performed under the auspices of the U.S. Department of Energy by Lawrence Livermore National Laboratory under Contract DE-AC52-07NA27344.

# Ignition and Growth Reactive Flow Model for IMX-101

Craig M. Tarver

Lawrence Livermore National Laboratory, 7000 East Avenue, Livermore, CA 94551, USA

**Abstract.** A set of Ignition and Growth (I&G) reactive flow model parameters is developed for the explosive IMX-101 containing DNAN, NQ, and NTO using the available shock initiation and detonation wave propagation experimental data. The unreacted equation of state for IMX-101 is based on experimental data from gas gun experiments by Furnish et al. and is similar to that of TNT. The product equation of state for IMX-101 is based on CHEETAH chemical equilibrium calculations and cylinder test experimental data. The IMX-101 reaction rate parameters are developed using hydrodynamic reactive flow simulations of several shock initiation and detonation experiments. One set of I&G parameters does a good job of reproducing both shock initiation and detonation experimental data. This is due to the fact that IMX-101 reacts over a relatively small pressure range from about 7 GPa to 20 GPa (C-J pressure). Advanced experiments using embedded gauges and/or laser interferometry could lead to better parameters.

## INTRODUCTION

The high explosive mixture IMX-101 containing 2,4-Dinitroanisole (DNAN), Nitroguanidine (NQ), and 3-Nitro-1,2,4-triazol-5-one (NTO) is designed to be a replacement for TNT, which has many safety, performance and environmental drawbacks. IMX-101 has been studied using several shock initiation and detonation tests, and sufficient experimental data exists to form a database for developing a predictive reactive flow model. IMX-101 is a relatively insensitive explosive that is generally used at an initial density of 1.63 – 1.64 g/cm<sup>3</sup>. Since its theoretical maximum density is 1.688 g/cm<sup>3</sup>, its initial porosity is usually 3.5%. IMX-101 has a measured unconfined failure diameter of between 8.128 and 8.509 cm. A sustained shock pressure of 8 GPa is required to produce shock to detonation transition (SDT) in about 3 cm of run distance. Several other detonation and shock initiation properties of IMX-101 have been measured, and all of the available data are used to develop a set of I&G parameters for IMX-101.

## THE IGNITION AND GROWTH REACTIVE FLOW MODEL

All reactive flow models require two equations of state, one for the unreacted explosive and another for its reaction products, and a reaction rate law for the conversion of the explosive to products. The Ignition and Growth (I&G) reactive flow model [1] uses two Jones-Wilkins-Lee (JWL) equations of state (EOS's):

$$p = A e^{-R_1 V} + B e^{-R_2 V} + \omega \square C_v T \quad (1)$$

where  $p$  is pressure,  $V$  is relative volume,  $T$  is temperature,  $\omega$  is the Gruneisen coefficient,  $C_v$  is the average heat capacity, and  $A$ ,  $B$ ,  $R_1$  and  $R_2$  are constants. These EOS's are fitted to unreacted Hugoniot and reaction product Hugoniot data. The three-term reaction rate equation is used:

$$\frac{dF}{dt} = I(1 - F)^b(\rho/\rho_0 - 1 - a)^x + G_1(1 - F)^c F^d p^y + G_2(1 - F)^e F^g p^z \quad (2)$$

$0 < F < F_{igmax}$                        $0 < F < F_{G1max}$                        $F_{G2min} < F < 1$

where  $F$  is the fraction reacted (actually the fraction of the chemical energy released),  $t$  is time in  $\mu$ s,  $\rho$  is the current density in g/cm<sup>3</sup>,  $\rho_0$  is the initial density, and  $p$  is pressure in Mbars.  $I$ ,  $G_1$ ,  $G_2$ ,  $a$ ,  $b$ ,  $c$ ,  $d$ ,  $e$ ,  $g$ ,  $x$ ,  $y$ ,  $z$ ,  $F_{igmax}$ ,  $F_{G1max}$ , and  $F_{G2min}$  are constants. Pressure and temperature equilibrium between the two phases is assumed.

The three-term rate law describes the three stages of reaction generally observed in shock initiation and detonation of heterogeneous solid explosives. For solid explosive detonation modeling, the first term of Equation (2) represents the ignition of the explosive as it is compressed by the leading 3D shock wave creating hot regions at the triple shock interactions. The fraction of explosive ignited is assumed to be equal to the void volume of the pressed explosive and reacts rapidly. For IMX-101 at 1.63 g/cm<sup>3</sup>, the initial void volume is 3.5%. The second reaction rate in Eq. (2) models the formation of the major gaseous reaction product gases (CO<sub>2</sub>, N<sub>2</sub>, H<sub>2</sub>O, CO, etc.). The third term in Eq. (2) is used to describe the relatively slow diffusion controlled formation of nanometer size solid carbon particles (diamond, graphite, or amorphous carbon) from single or small groups of carbon atoms. For IMX-101, the last 30% of the chemical energy release is assumed to be due to solid graphite nanoparticle formation in a diffusion controlled process. This assumption has worked well for modeling the carbon rich explosives TNT and TATB.

For solid explosive shock initiation modeling, the first term of Eq. (2) again represents the ignition of the explosive as it is compressed by the leading shock wave creating “hot spots” that can react and grow or fail to grow. The fraction of explosive ignited for IMX-101 is 3.5%. The second reaction rate in Eq. (2) models the growth of the reacting “hot spots” as they consume the neighboring shock heated material. The third term in Eq. (2) describes the coalescence of the growing hot spots and the rapid transition to detonation that consumes any remaining unreacted explosive. Generally different sets of I&G parameters are needed to model the time resolved details of shock initiation and detonation, because they are driven by two different physical processes occurring at very different pressures. However, since IMX-101 requires 7 to 8 GPa shock pressures for shock initiation and only produces 20 GPa when detonating, it was possible to match the available experimental data on IMX-101 with one set of I&G parameters. Table 1 lists these I&G parameters for IMX-101. If more time resolved experimental data is measured, the modeling of the two reactive flow processes can be more fully refined.

**Table 1.** Ignition and Growth model parameters for IMX-101 at an initial density of  $\rho_o = 1.63 \text{ g/cm}^3$

Unreacted JWL EOS	Product JWL EOS	Reaction rate parameters
A = 211.25 Mbar	A = 7.630831 Mbar	I = 20000 $\mu\text{s}^{-1}$ a = 0.0 x = 4.0                      b = 0.667
B = -0.043396 Mbar	B = 0.307363 Mbar	F <sub>igmax</sub> = 0.035 F <sub>G1max</sub> = 0.7              F <sub>G2min</sub> = 0.7
R <sub>1</sub> = 9.8	R <sub>1</sub> = 5.5064	G <sub>1</sub> = 625 Mbar <sup>-3</sup> $\mu\text{s}^{-1}$ c = 0.667                      d = 0.667
R <sub>2</sub> = 0.98	R <sub>2</sub> = 2.0	y = 3.0
$\omega$ = 0.5675	$\omega$ = 0.4536	G <sub>2</sub> = 3.125 Mbar <sup>-1</sup> $\mu\text{s}^{-1}$
Cv = 2.70386e-5 Mbar/K	Cv = 1.0e-5 Mbar/K	z = 1.0
To = 298K	Eo = 0.06204 Mbar-cm <sup>3</sup> /cm <sup>3</sup> -g	e = 0.667                      g = 0.667

## COMPARISONS BETWEEN EXPERIMENTS AND CALCULATIONS

### 1. IMX-101 unreacted equation of state

Furnish et al. [2] performed five planar impact gas gun experiments at shock pressures from 4 to 16 GPa on various thickness target targets of IMX-101. The experimental diagnostic was PDV or VISAR, which measured the interface particle velocity between the IMX-101 and a NaCl or LiF window. The initial measured particle velocity was assumed to be due to unreacted IMX-101, the shock velocity was also measured, and the shock pressure calculated. Figure 1 shows the five measured shock velocity versus particle velocity states for “unreacted” IMX-101, along with the I&G unreacted Hugoniot states calculated by setting I = G<sub>1</sub> = G<sub>2</sub> = 0 in Eq. (2). Figure 2 shows the related shock pressure versus particle velocity states. The agreement is good, considering the assumptions made in the experiments. These unreacted Hugoniot states are also close to measurements on TNT and other similar explosives.

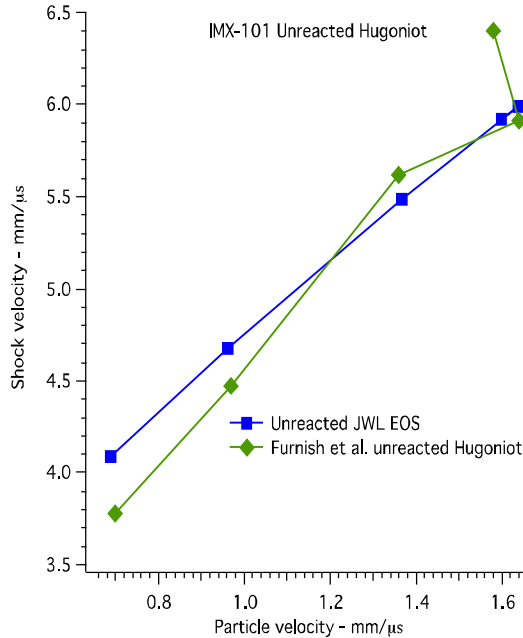


Figure 1. Unreacted IMX-101 shock velocity versus particle velocity states

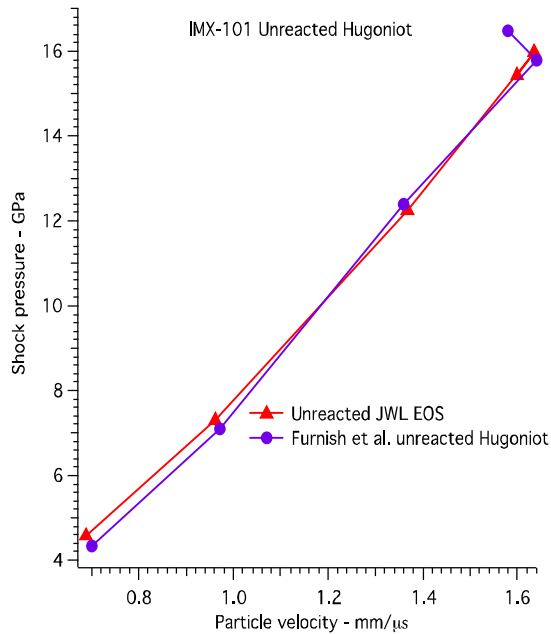


Figure 2. Unreacted IMX-101 shock pressure versus particle velocity states

## 2. IMX-101 reaction product equation of state

The CHEETAH chemical equilibrium code [3] was used to calculate the C-J state and product expansion states for 1.63 g/cm<sup>3</sup> IMX-101. The calculated infinite diameter C-J detonation velocity was 7.189 mm/μs, and the C-J pressure was 0.2089 Mbar. Of course, these values cannot be reached in finite diameter charges of IMX-101. Measured IMX-101 detonation velocities in finite diameter charges are approximately 6.9 mm/μs. The CHEETAH JWL EOS fitting routine produced the product JWL EOS listed in Table 1. Three 10.16 cm inner diameter IMX-101 loaded copper cylinder tests were fired at ARL. The measured copper wall displacements are compared to the I&G calculated copper wall displacement history using the IMX-101 parameters listed in Table 1 are shown in Fig. 3. The three measured wall displacement histories agree well with the 2D hydrodynamic calculated displacement history. The I&G calculated copper free surface velocity history is shown in Fig. 4. Approximate copper wall velocities obtained by taking derivatives of the measured displacements agree fairly well with the calculated wall velocity history shown in Fig. 4. Therefore the IMX-101 reaction product JWL EOS fitted to CHEETAH C-J state and expansion calculations is appropriate for use in the I&G reactive flow model.

These cylinder tests on IMX-101 were fired at an initial temperature of -20°C in 2013, rather than at ambient temperature (25°C). The IMX-101 data package included one ambient temperature cylinder test from 2009, but the wall motion data on the two sides of the cylinder did not agree. Both sets of data were close to the calculated wall velocities in Fig. 4. Only TATB-based explosives of all the major solid explosives show substantial initial temperature dependences on shock initiation and detonation performance. These dependences are due to TATB's large thermal expansion coefficient, its large thermal diffusivity, and its large activation energy barrier for decomposition. These relevant properties of IMX-101 have not been measured, but it is unlikely that its detonation propagation has a large dependence on initial temperature.

## 3. The unconfined failure diameter of IMX-101

The unconfined failure diameter was measured using 50 cm long cylinders of IMX-101 initiated by 10 cm long Composition B booster charges. Since Comp B has a higher C-J pressure than IMX-101, the initial IMX-101 waves

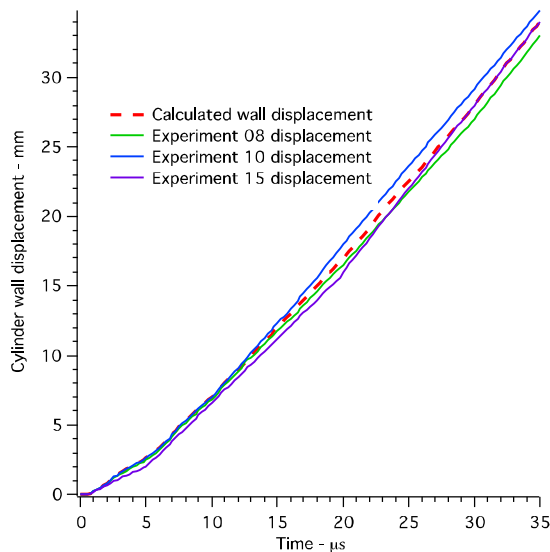


Figure 3. Copper cylinder wall displacement histories for three cylinder tests and the I&G calculation

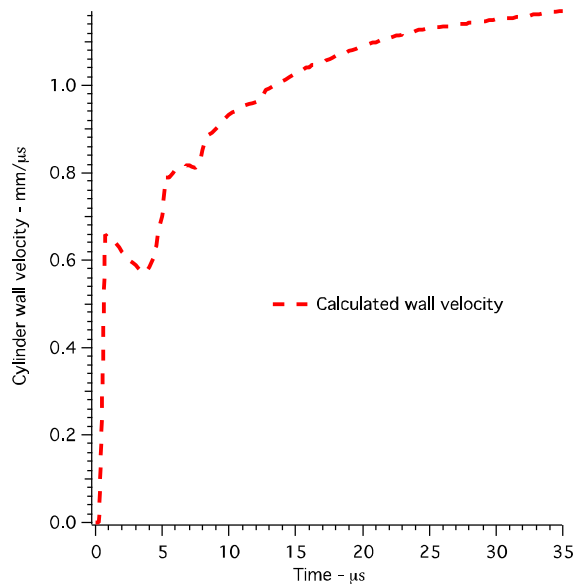


Figure 4. Calculated copper cylinder velocity history using the IMX-101 I&G model parameters in Table 1.

were overdriven and took about 10 cm to slow down to their steady detonation velocity. After that occurred, the detonation velocity in an 8.128 cm diameter cylinder of IMX-101 slowly continued to decrease for another 10 - 15 cm until the detonation failed. An 8.509 cm diameter IMX-101 cylinder continued to propagate a steady velocity detonation wave at about 6.5 mm/ $\mu$ s to the end of the charge. Thus the unconfined IMX-101 cylindrical failure diameter is greater than 8.128 cm and less than 8.509 cm. I&G modeling of these two diameters was conducted, and the values of the  $G_1$  and  $G_2$  coefficients were varied until the 8.128 cm charge failed and the 8.5 cm charge continued to detonate. The final values of  $G_1$  and  $G_2$  are listed in Table 1. For diameters close to failure, the detonation wave velocity is much lower than the C-J velocity, and the wave front is curved. Figure 5 shows the curvature of the calculated IMX-101 detonation wave front at 70  $\mu$ s as pressure fringes (left hand side) and the fraction of the chemical energy released fringes (right hand side).

The calculated IMX-101 unconfined detonation wave curvature in Fig. 5 is approximately 1.25 cm, and the reaction zone length for complete reaction is greater than 2 cm. The unconfined detonation wave curvature was not measured in these experiments. The IMX-101 detonation wave traveled 38 cm in 58  $\mu$ s for an average detonation velocity of 6.55 mm/ $\mu$ s. The IMX-101 was initially overdriven by the Comp B detonation wave so the steady detonation velocity reached in the IMX-101 is slightly less than 6.55 mm/ $\mu$ s. Since the failure diameter of IMX-101 is so large compared to other solid explosives, it was important to obtain the correct calculated unconfined failure diameter of IMX-101 before modeling the other detonation and shock initiation experiments.

#### 4. Confined IMX-101 detonation wave curvature experimental data and I&G calculations

Although no unconfined detonation wave curvature data is available, heavily confined IMX-101 detonation velocity and wave curvature data has been reported using the instrumented Expanded Large Scale Gap Test (iELSGT). The detonation velocity is measured at several pin locations in a steel wall confining a 15.2 cm cylindrical IMX-101 charge initiated by 9.5 cm of 1.56 g/cm<sup>3</sup> Pentolite, and the wave curvature is measured at the end of the IMX-101 charge. Figure 6 shows the detonation velocity measurements (left side) and the curvature measurements (right side) for five experiments, three at cold and two at ambient temperatures. Figure 7 shows the corresponding I&G calculation close to breakout at the end of IMX-101 charge using pressure fringes (top) and fraction of the energy released fringes (bottom). The calculated IMX-101 detonation velocity for the 15.2 cm long charge is 6.64 mm/ $\mu$ s, in good agreement with the measurements in Fig. 6, and the calculated wave curvature is between 2 and 3 mm, in good agreement with the 2 mm lag measurement, which ends at 28 mm radius, in Fig. 6.

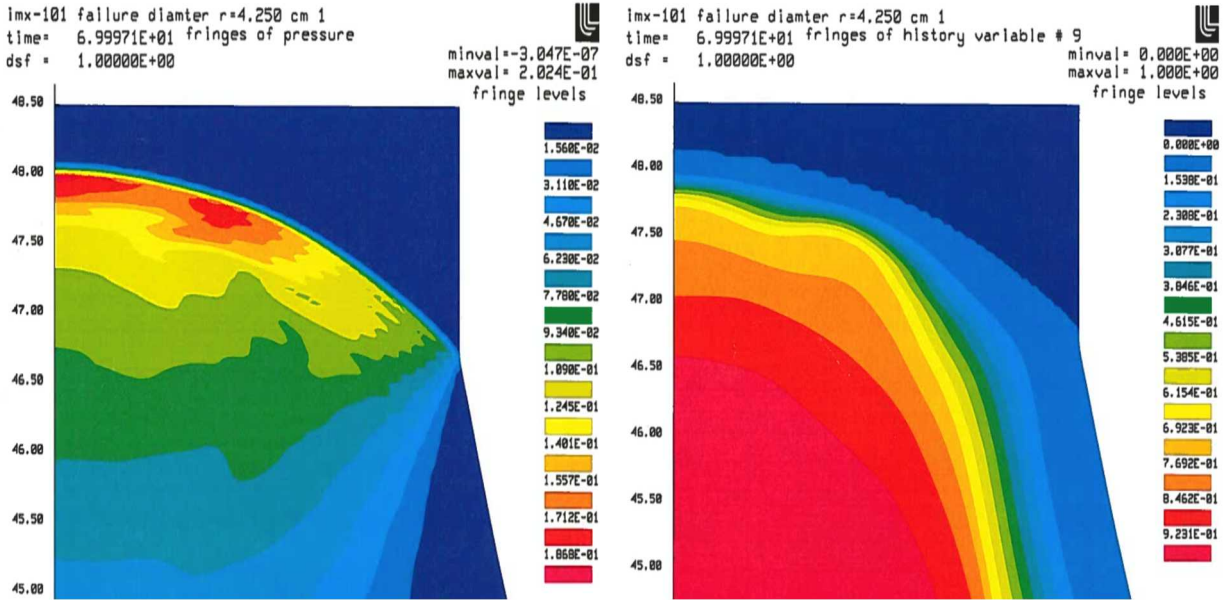


Figure 5. Pressure (left) and fraction of the chemical energy released (right) fringes for a 8.50 cm diameter cylinder of detonating IMX-101 at time = 70  $\mu$ s.

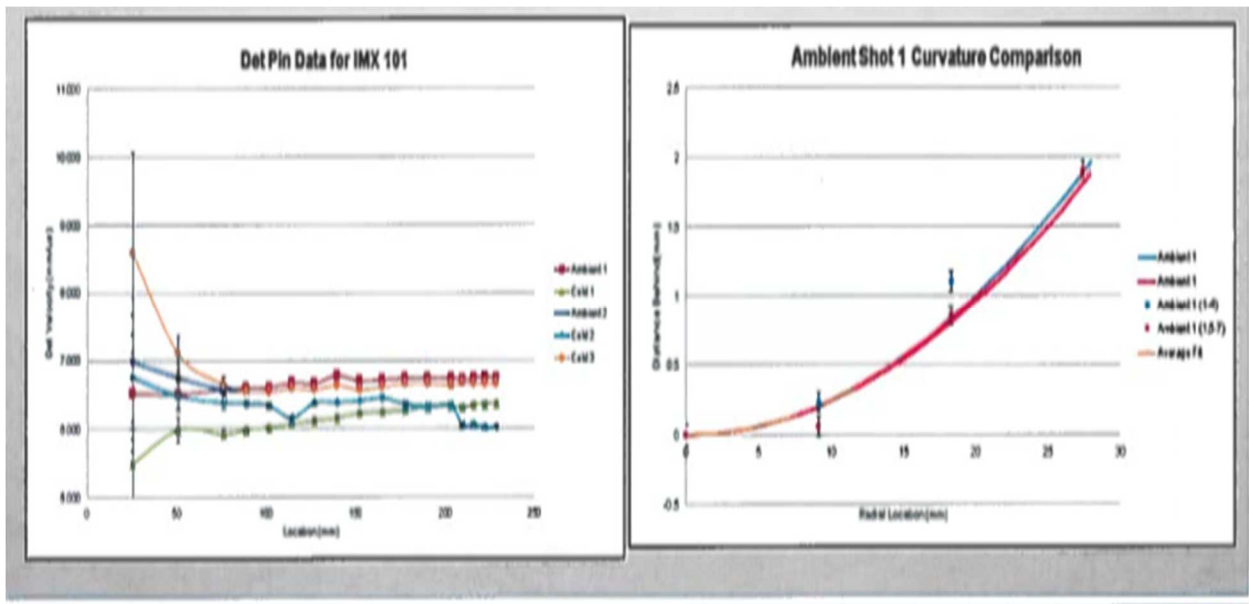


Figure 6. Experimental data for IMX-101 detonation velocity (left) and wave curvature (right)

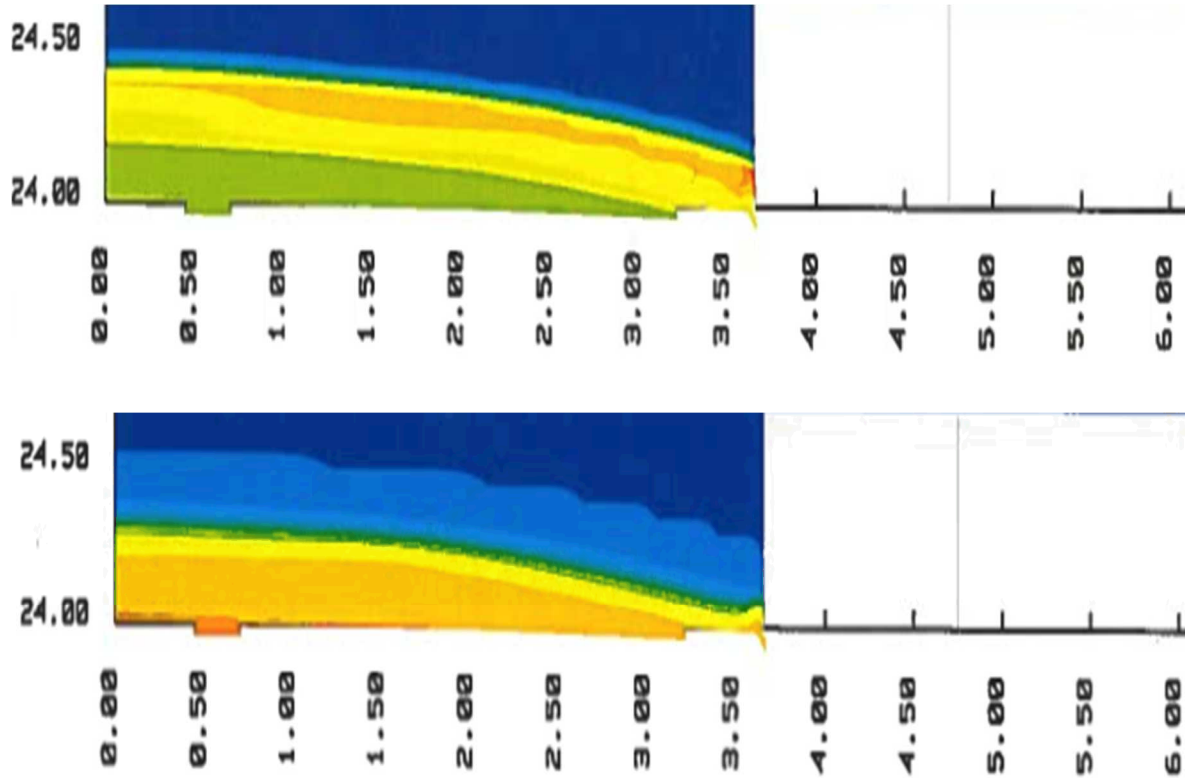


Figure 7. I&G calculated pressure (top) and fraction reacted (bottom) fringes for IMX-101

##### 5. IMX-101 detonation corner turning test and modeling results

The final IMX-101 detonation comparison is based on a detonation corner test based on the ELSGT geometry with a 15.24 cm diameter by 12.7 cm long IMX-101 charge placed under the usual ELSGT setup, except that a copper wall was used instead of steel. Since insensitive high explosives like IMX-101 and LX-17 (92.5% TATB/7.5% Kel-F binder) have long reaction times, a rapid change in the charge geometry can create rarefaction waves that lower the reaction rates and cause “dead zones” of zero or incomplete reaction and even complete failure of the detonation wave. It is important know how much chemical energy is lost in this type of process and determine the correct initiation conditions so that the detonation wave continues to propagate. Fiber optic cables are placed along the sides and top of the 12.7 cm long IMX-101 charge to determine the arrival times of the spreading detonation wave. Figure 8 shows the test geometry (left side) with the detonator/booster on top and the IMX-101 acceptor charge below and the detonation wave breakout (right side) as the diverging detonation wave spreads toward the outer boundary of the acceptor charge. On the right hand side of Fig. 8, the light from the IMX-101 acceptor charge shows that the detonation wave requires a long propagation time and distance to reach the edge of the acceptor charge. The 2D axi-symmetric I&G simulation of the first breakout of this IMX-101 detonation wave is shown in Fig. 9 at a time of 52  $\mu$ s from initiation. The pressure fringes are shown on the left side, and the fraction of chemical energy release fringes are shown on the right. The detonation wave in the acceptor IMX-101 charge begins to shrink initially and then requires over 10 cm and 16  $\mu$ s to grow outward to the edge of the acceptor charge. The shape of the calculated detonation wave front is similar to the experimental shown in Fig. 8, but an exact comparison requires the experimental fiber optic arrival times, which were not available.

This is all of the available experimental data on detonation wave propagation in IMX-101. The following sections discuss I&G modeling of the available shock initiation data on IMX-101.

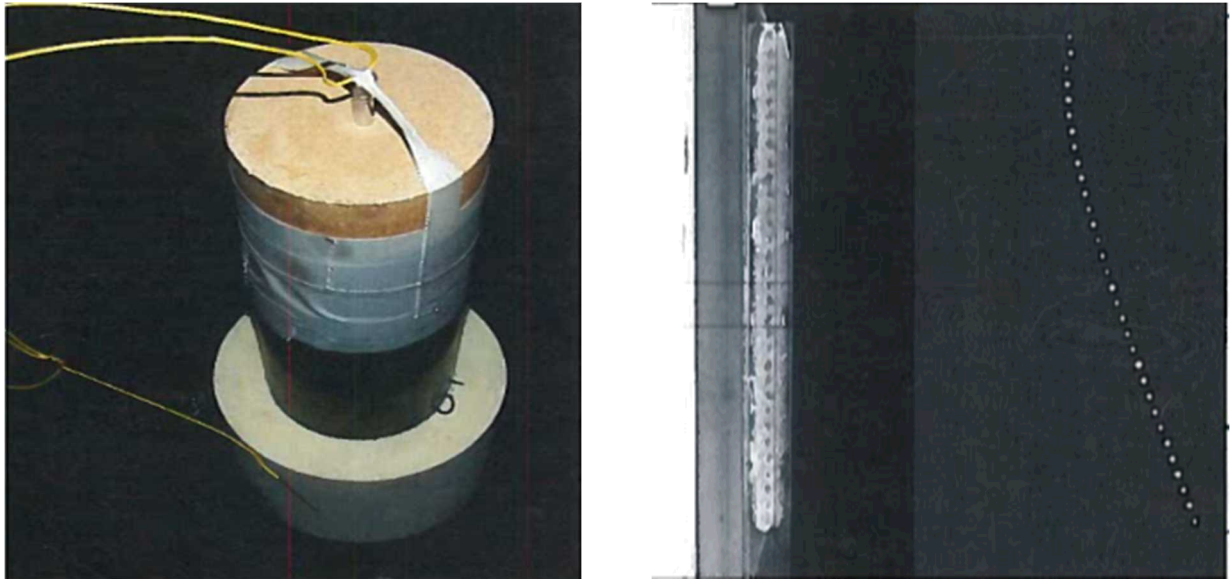


Figure 8. Detonation corner turning test geometry (left – booster on top) and detonation wave breakout results (right – booster on top but not shown), IMX-101 acceptor shown on left, and breakout light shown on right)

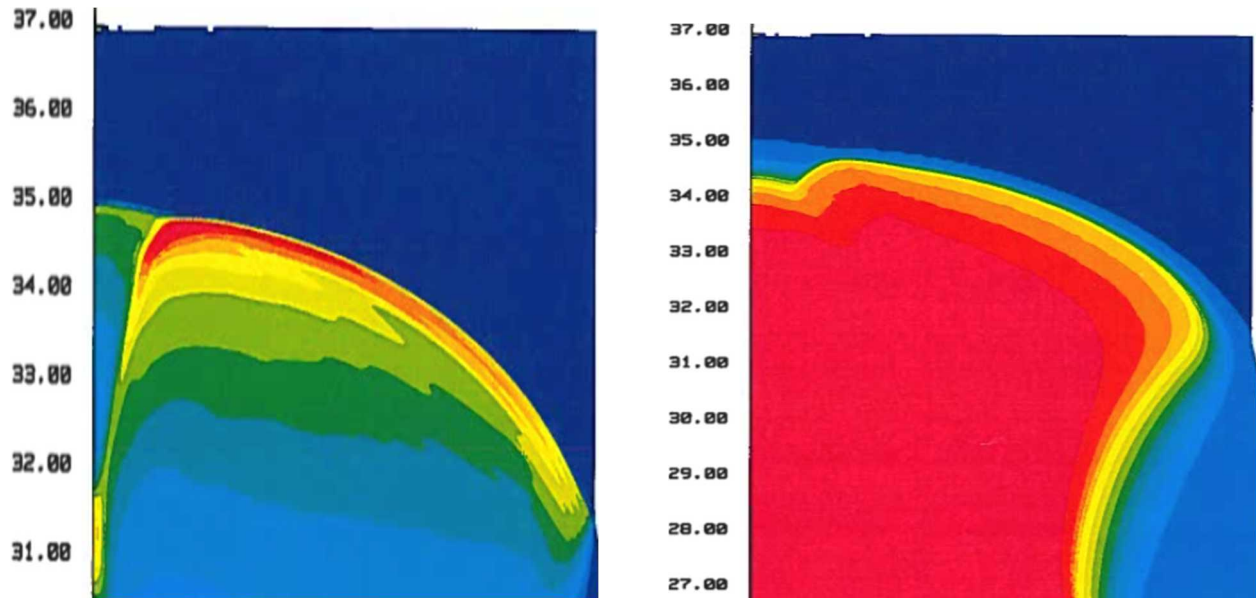


Figure 9. I&G calculated pressure fringes (left) and fraction reacted fringes (right) at 52  $\mu$ s from initiation. The maximum pressure equals 23.3 GPa, and the detonation wave has propagated  $\sim$ 10 cm into the acceptor cylinder. The fraction reacted fringes show that a large volume of partially reacted IMX-101 exists behind the expanding wave.

## 6. Time resolved particle velocity growth in planar impact experiments on IMX-101

Furnish et al. [2] performed 20 planar impact gas gun shots at 5 shock pressures from 4 to 16 GPa on 3, 6, 9 and 12 mm thick IMX-101. The interface particle velocity history at the IMX-101 and a NaCl or LiF window boundary was measured using PDV or VISAR. The experimental geometries were modeled using the I&G reactive flow model parameters listed in Table 1. Figures 10 – 14 show the comparisons in order of increasing shock pressure.

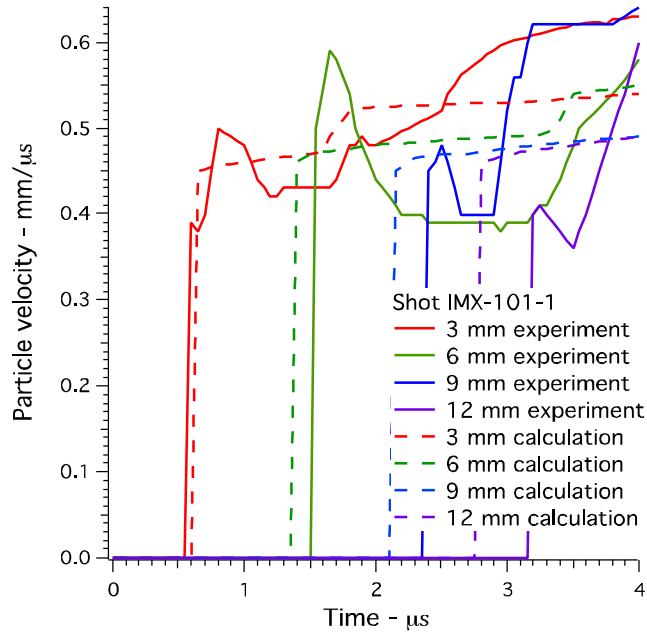


Figure 10. Experimental and calculated particle velocity histories for IMX-101 impacted at ~4.3 GPa

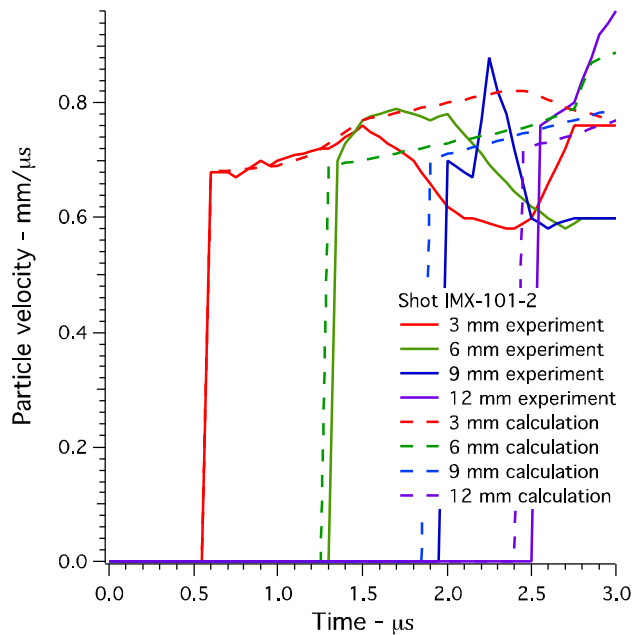


Figure 11. Experimental and calculated particle velocity histories for IMX-101 impacted at ~7.1 GPa

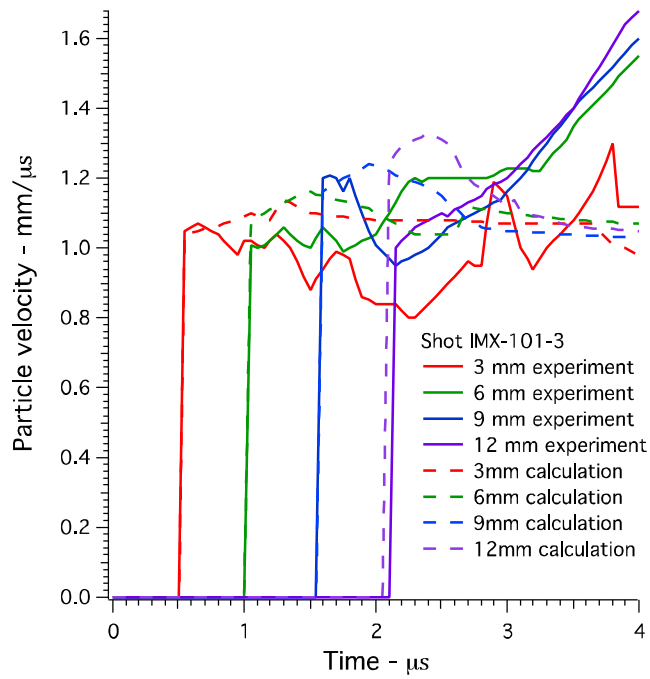


Figure 12. Experimental and calculated particle velocity histories for IMX-101 impacted at ~12.4 GPa

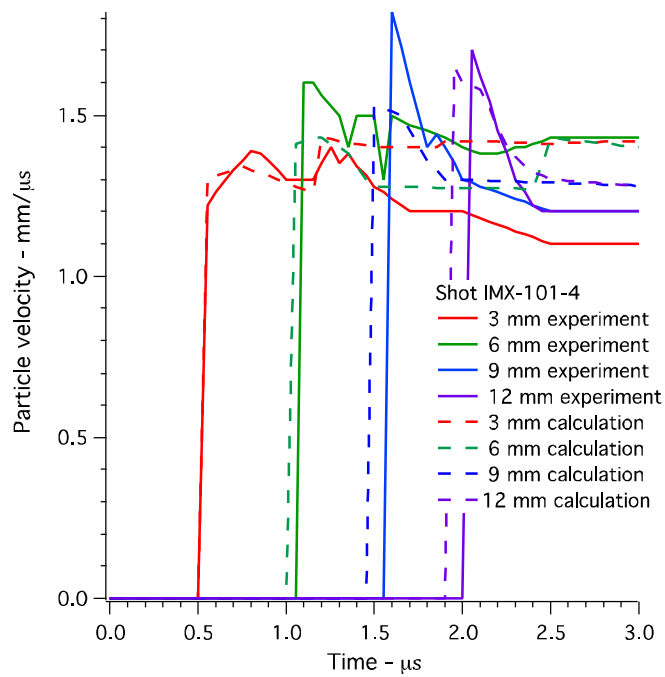


Figure 13. Experimental and calculated particle velocity histories for IMX-101 impacted at ~15.8 GPa

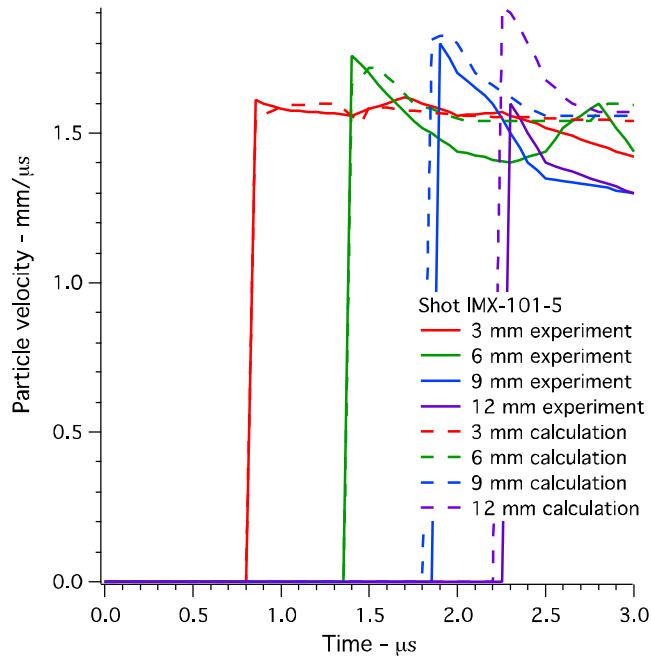


Figure 14. Experimental and calculated particle velocity histories for IMX-101 impacted at ~16.5 GPa

The agreement between the experimental and calculated particle velocity histories in Figs. 10 – 14 are good, and the shock to detonation transitions (SDT) in Figs. 13 and 14 occurred at the correct gauge positions (9 mm in Fig. 13 and 6 mm in Fig. 14). The experimental records in Figs. 10 – 12 did not show SDT but did exhibit some particle velocity increases behind the shock fronts. The calculations in Figs. 10 – 12 showed similar particle velocity increases due to exothermic chemical reactions.

#### 7. Run distance to detonation versus shock pressure (Pop Plot) SDT experiments and calculations

Five run distance to detonation versus shock pressure SDT results are available for IMX-101 in a wedge test geometry. The wedge test is a 2D experiment that uses an explosive driver system that does not maintain a constant pressure behind the leading shock front. The measured run distances to detonation can be affected by both rear and side rarefaction wave induced effects. However, it is the classical way to represent SDT so it is included here. Figure 15 contains five wedge test results plus the two shots by Furnish et al. that detonated. I&G calculated run distances to detonation for sustained shock pressures produced by aluminum flyer plates of various velocities are included in Fig. 15 for comparison. There is a large uncertainty in the experimental data, but it is not very different from the I&G calculations. The reported 3 mm run distance to detonation at a shock pressure of 17 GPa may be in error. Therefore this Pop Plot for IMX-101 is good enough for approximate SDT estimations.

#### 8. Expanded Large-Scale Gap Test (ELSGT) results for IMX-101

The shock sensitivity of IMX-101 was measured in the ELSGT by varying the thickness of the PMMA attenuator layer to measure a failure to detonate versus detonation threshold thickness of 158 “cards” or 4.01 cm of PMMA. The ELSGT geometry was modeled exactly in two dimensions using the I&G parameters in Table 1. A 4 cm thick PMMA layer was predicted to produce SDT in the IMX-101, while a 4.5 cm thick PMMA layer caused failure of detonation. This result represents another qualitative check on the accuracy of the I&G parameters.

#### 9. Quantitative ELSGT Pentolite booster with a 5.59 mm PMMA attenuator “Cutback” SDT Experiment

The final experiments on IMX-101 are run distance to detonation measurements taken using the ELSGT 9.5 cm long, 1.56 g/cm<sup>3</sup> Pentolite booster, a 5.59 mm thick PMMA attenuator, various thicknesses of IMX-101 from 5 to

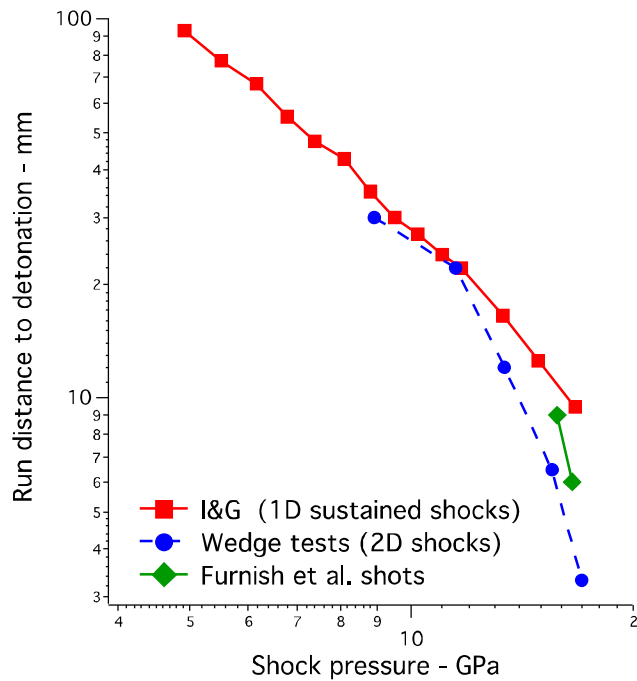


Figure 15. Experimental and calculated run distances to detonation versus shock pressure for IMX-101

30 mm, and PDV interface velocity measurements through PMMA windows attached to the rear of the IMX-101 charges. These experiments measure the SDT process at high shock pressures and clearly show the gradual development of a detonation wave as the thickness of IMX-101 increases. The experiments using 5, 10, and 15 mm of IMX-101 are still shock initiating when the shocks reach the PMMA windows, and the experiments using 20, 25, and 30 mm of IMX-101 transition to detonation before the shock waves reached the PMMA windows. Figure 16 contains the six experimental IMX-101/PMMA interface particle velocity histories and the six corresponding I&G calculations. The actual experimental arrival times are not known, so the calculated times between Pentolite initiation and the shock wave arrivals at the IMX-101/PMMA interface are used. The calculations also show that detonation is achieved for the 20, 25, and 30 mm thick IMX-101 charges, but not for the 5, 10, and 15 mm thick charges. Good agreement between the experimentally measured and calculated shock states and subsequent energy release rates for all six experiments.

## CONCLUSIONS

The available experimental shock initiation and detonation data on IMX-101 was simulated using the Ignition and Growth reactive flow model. The model parameters were based on unreacted Hugoniot data, cylinder test data, unconfined failure diameter data, and data from several other experiments that measured the chemical energy release rates under different shock scenarios. Since the shock initiation and detonation pressures are not very different one set of I&G parameters was found that reproduces fairly well both shock initiation and detonation experimental results. More accurate I&G shock initiation parameters require more sophisticated, time resolved experiments employing embedded manganin pressure and/or aluminum particle velocity gauges. To ensure reliable predictions of high shock pressure, short pulse duration initiation schemes, electric gun experiments are needed to measure the threshold conditions for initiation of detonation versus failure to initiate. To better understand the performance of detonating IMX-101, time resolved measurements of the reaction zone structure using embedded gauges, the acceleration of thin metal plates using PDV, and/or the interaction of the IMX-101 detonation waves with transparent windows using PDV-type techniques are required. However, the IMX-101 I&G parameters in Table 1 will allow performance and safety scenarios to be calculated right away with good confidence.

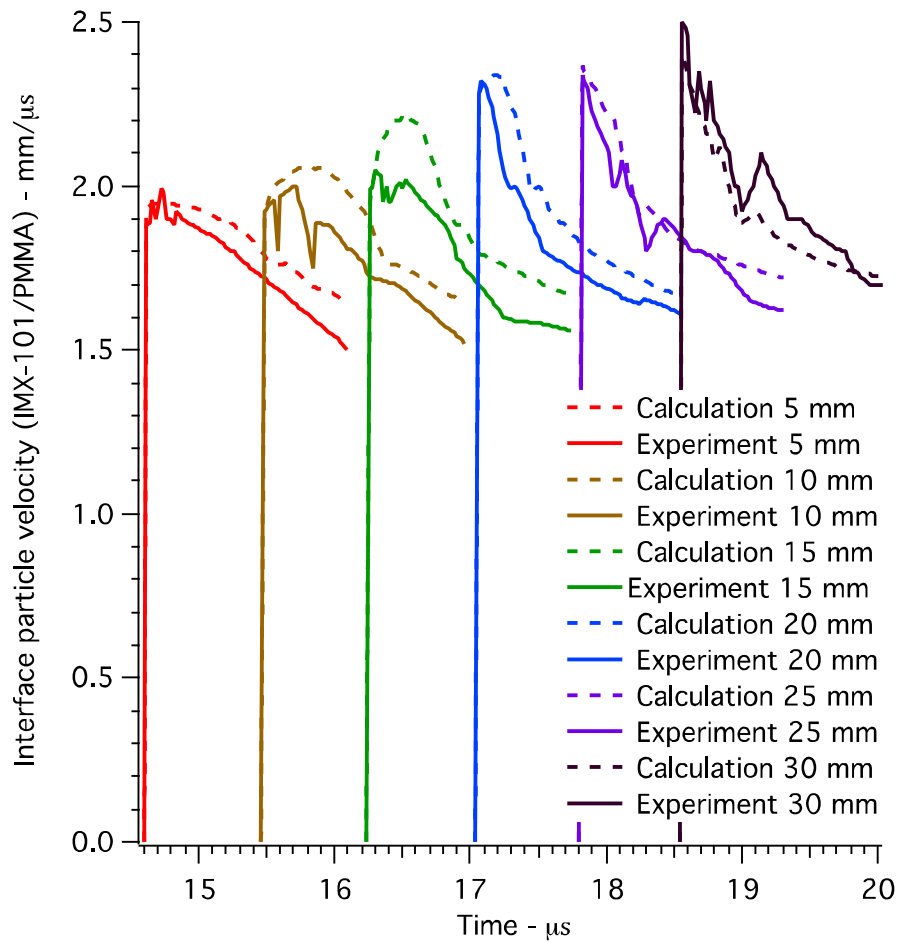


Figure 16. Experimental and calculated interface particle histories between various thicknesses of IMX-101 and PMMA windows following shock initiation by 9.5 cm of Pentolite

## REFERENCES

1. C. M. Tarver et al. four recent papers in the *Fifteenth International Detonation Symposium*, Office of Naval Research ONR-43-280-15, San Francisco, CA, July13-18, 2014, p. 284, 333, and 620.
2. M. D. Furnish, S. Root, and P. Samuels, *ibid.*, p. 1543.
3. K. S. Vandersall, F. Garcia, L. E. Fried, and C. M. Tarver, *ibid.*, p. 255.